Measurement of coefficients of the Ginzburg-Landau equation for patterns of Taylor spirals

Afshin Goharzadeh*
Mechanical Engineering Department, The Petroleum Institute, P.O. Box 2533, Abu Dhabi, United Arab Emirates

Innocent Mutabazi†
Laboratoire d'Ondes et Milieux Complexes (LOMC), FRE 3102, CNRS–Université du Havre, 25 rue Philippe Lebon, BP 540, F-76058 Le Havre Cedex, France
(Received 25 March 2010; published 13 July 2010)

Patterns of Taylor spirals observed in the counter-rotating Couette-Taylor system are described by complex Ginzburg-Landau equations (CGLE) and have been investigated using spatiotemporal diagrams and complex demodulation technique. We have determined the real coefficients of the CGLE and their variations versus the control parameters, i.e., the rotation frequency of cylinders.

DOI: 10.1103/PhysRevE.82.016306 PACS number(s): 47.20.Ky, 47.27.Cn

I. INTRODUCTION

The hydrodynamic stability of flows within rotating coaxial cylinders (Couette-Taylor system) have been extensively reported over the past decades, both from experimental as well as from theoretical or numerical points of view [1–3]. Annular flows with rotating cylinders contribute to the understanding of transition to turbulence in shear flows in closed systems. These flows are encountered in many industrial applications, such as flow separation processes or drilling operations in the petroleum industry. In the counter-rotating Couette-Taylor system, centrifugal instability generates intriguing mechanism of the transition to turbulence, from the circular Couette flow, through spirals and interpenetrating spirals to intermittent flow [4–6] and turbulent spirals [7–12]. Interpenetrating spirals (IPS) propagate axially in opposite directions with finite velocity and are good prototypes of interacting nonlinear waves with a large group of symmetries [1,13,14]. The properties of spiral vortices have been investigated using theoretical methods of group theory and numerical simulations [2,15–18], however, few experimental studies have focused on the characteristics of spirals and interpenetrating spirals [1,19], because of their three dimensional character which renders their analysis and observation very difficult. Interaction between left and right spirals may generate remarkable spatiotemporal pattern containing a rich variety of coherent structures such as sources, holes, defects, and sinks. Therefore, the dynamics of single spirals and interpenetrating spirals can be described in the framework of amplitude equations [20,22]. Near the threshold the form of the amplitude equation depends on the symmetries and the nature of primary bifurcation. The Complex Ginzburg-Landau equation (CGLE) describes a variety of dynamical patterns observed in many hydrodynamic flows [20,22,23,25–27]. The values of its coefficients depend on the system parameters and vary from one system to another. Many theoretical and numerical studies of the CGLE in its scaled form have been recently performed leading to a rich variety of states and coherent structures. The applicability of such a general equation to a given experiment requires an appropriate experimental determination of CGLE coefficients. This has been performed for thermal convection in mixtures by Kolodner *et al.* [28,29] and for hydrothermal waves by Burguette *et al.* [30].

In this paper, we report experimental results of the transition from circular Couette flow to spirals and Interpenetrating Spirals and focus our attention on the properties of IPS flow have not been reported before. We have determined the amplitude, frequency and wave number of spirals using a complex demodulation technique [31]. Assuming that these patterns can be described by the theory of Ginzburg-Landau Eqs. [24,25], we have determined the corresponding real coefficients using a method developed by Burguette *et al.* [30]. The paper is organized as follows: in Sec. II, we describe the experimental setup and procedure, in Sec. III, we present the spiral and IPS patterns, the adequateness of the Giznburg-Landau equations for their description and the method of coefficient extraction. Results are presented in Sec. IV. The paper ends with a discussion and conclusion.

II. EXPERIMENTAL SETUP

The Couette-Taylor configuration used in our experiment has been described in [6]. It consists of two coaxial horizontal counter-rotating cylinders. The inner cylinder is made of black Delrin with a radius $a=4.459$ cm. The outer cylinder is made of transparent plexiglass with a radius $b=5.050$ cm. The gap between the cylinders is $d=b-a=0.591$ cm over a working length $L=27.5$ cm. Hence, the system has a radius ratio $\eta=a/b=0.883$, and an aspect ratio $\Gamma=L/d=46$, and it can be considered as an extended flow system. In our experiment, rigid end plates are attached to the outer cylinder. The cylinders are driven independently in opposite directions by two DC servomotors. Thus the control parameters of the Couette-Taylor system are the Reynolds numbers defined for the inner and outer cylinders respectively: $R_i=\Omega_i a d/\nu$ and $R_o=\Omega_o b d/\nu$, where Ω_i and Ω_o are angular frequencies of inner and outer cylinder respectively and ν the kinematic viscosity of the fluid. We have used distilled water at $T=21$ °C with 2% Kalliroscope $AQ1000$

*agoharzadeh@pi.ac.ae
†mutabazi@univ-lehavre.fr

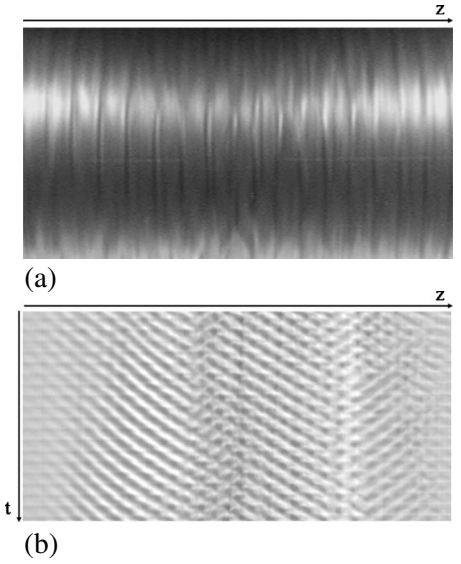

FIG. 1. Pattern of Interpenetrating Spirals (a) photography, (b) spatiotemporal diagram, for $R_0=-1375$ and $\varepsilon R_i=520$.

suspension for visualization. With a light from a fluorescent tube, the flow was visualized from the front side. To obtain spatial information about the flow dynamics, a linear 1024-pixel charge-coupled device (CCD) array recorded the intensity distribution $I(z)$ of the light reflected by Kalliroscope flakes from a line along the axis at the middle of the cylinders. The recorded length was from 20 to 25 cm in the central part of the system [Fig. 1(a)], corresponding to a spatial resolution of 41 to 51 pixels/cm. The intensity was sampled at 256 values, displayed in gray levels at regular time intervals along the time axis to produce space-time diagrams $I(z,t)$ of the pattern [Fig. 1(b)]. The complex demodulation technique [31] was applied in order to extract some spatial and temporal properties of the pattern. The dynamics of patterns is investigated using the reduced control parameter $\varepsilon=(R_i-R_{ic})/R_{ic}$ where R_{ic} is the critical value of the inner Reynolds number.

III. SPIRALS AND INTERPENETRATING SPIRALS

In our counter-rotating Couette-Taylor system and for a fixed external Reynolds number $R_o<-1200$, the first bifurcation occurs at R_{ic} (which depends on R_o) and gives rise to a pattern of propagating helicoidal vortices named spirals. Above the onset, because of the large axial extent of the system, left and right propagating spirals appear separated by a source [Fig. 2(a)]. The source is an "active" coherent structure, which sends out waves to both directions with approximately the same frequencies and wave numbers. The source appears randomly in the pattern at any positions which may change when the control parameter is varied abruptly. For $(\varepsilon>0)$, the lifetime of the source is short because the left and right spirals interact nonlinearly, invade each other [Fig. 2(b)] and lead to interpenetrating spirals [Fig. 2(c)]. For $\varepsilon=0.012$, the lifetime of the source is approximately 60 s. During this short period, spirals vanish slightly in space before reaching the ends of the system, suggesting that the IPS

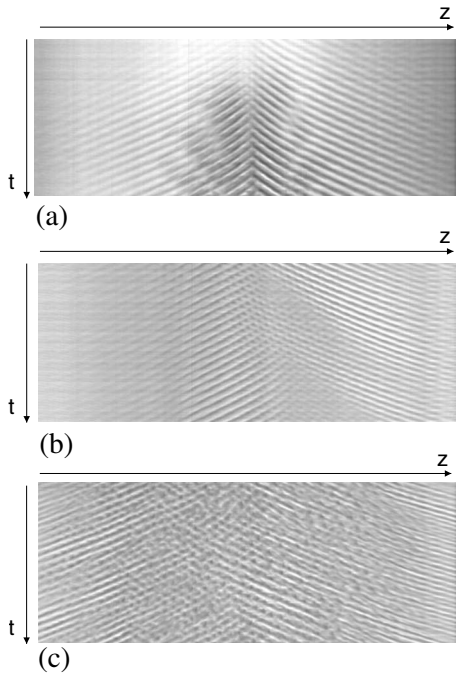

FIG. 2. Spatiotemporal diagram of counter-propagating spirals and interpenetrating spirals for a fixed outer Reynolds number $R_o=-1200$. (a) $R_i=486$ or $\varepsilon=0.012$; (b) $R_i=490$ or $\varepsilon=0.02$; and (c) $R_i=501$ or $\varepsilon=0.04$.

pattern has soft boundaries near the threshold (no reflection from the boundaries). The increase of the inner Reynolds number (or ε) reduces considerably the lifetime of the source. Figure 2(b) shows a typical spatiotemporal diagram of IPS at an early stage of their life just after that source disappeared from the system. Three regions are clearly observed. Two regions in left and right side of the diagram contain only left or right spirals, respectively. A third region in the middle contains left and right spirals traveling in opposite directions. As the control parameter increases the region of interpenetrating spirals increases in size. Figure 2(c) shows the space-time diagram for $\varepsilon=0.04$ in which very complex structures are observed. The structure of the spirals and IPS patterns depends on two control parameters, the inner and outer Reynolds numbers R_i and R_o, respectively. In order to simplify the presentation, we will describe the dynamics of interpenetrating spirals for fixed values of the outer Reynolds number $R_o=-1200$, -1500, and -2000 and increasing values of R_i.

A. Complex Ginzburg-Landau equations (CGLE)

The signal of the interpenetrating spirals in an extended Couette-Taylor system can be represented as follows [32]:

$$I(z,t)=\mathrm{Re}[A(z,t)e^{i[qz-\omega t+m\theta]}+B(z,t)e^{i[qz+\omega t-m\theta]}] \quad (1)$$

where $\mathrm{Re}(x)$ represents the real part of the quantity (x), $A(z,t)$ and $B(z,t)$ are the amplitudes of right and left traveling spirals, ω is the frequency, m is the azimuthal wave number, q is the axial wave number. As the spiral pattern appears through a supercritical Hopf bifurcation, the amplitudes

$A(z,t)$ and $B(z,t)$ of the opposite traveling waves can be described by the coupled complex Ginzburg-Landau equations [26,33]:

$$\tau_0\left(\frac{\partial A}{\partial t}+v\frac{\partial A}{\partial z}\right)=\varepsilon(1+ic_0)A+\xi_0^2(1+ic_1)\frac{\partial^2 A}{\partial z^2}-g(1+ic_2)|A|^2A-\delta|B|^2A, \quad (2)$$

$$\tau_0\left(\frac{\partial B}{\partial t}-v\frac{\partial B}{\partial z}\right)=\varepsilon(1+ic_0)B+\xi_0^2(1+ic_1)\frac{\partial^2 B}{\partial z^2}-g(1+ic_2)|B|^2B-\delta|A|^2B, \quad (3)$$

where τ_0 is the characteristic time, v the axial group velocity, ε control parameter and ξ_0 the coherence length, g the nonlinear saturation coefficient, δ the coupling coefficient, c_0 is the linear correction to the frequency, c_1 and c_2 represent linear and nonlinear dispersion coefficients of the waves. For the stability of IPS, $\delta \ll g$, i.e., the coupling is not destructive but allows a coupling at any position. The complex Ginzburg-Landau equations have solutions of the form:

$$A(z,t)=|A(z,t)|e^{i(q_pz-\omega_pt)} \quad (4)$$

$$B(z,t)=|B(z,t)|e^{i(q_pz+\omega_pt)} \quad (5)$$

where q_p and ω_p are wave number and frequency of perturbations. The real amplitudes $|A(z,t)|$ and $|B(z,t)|$ are experimentally obtained. The Eqs. (4) and (5) are substituted in Eqs. (2) and (3) in order to separate the real and imaginary parts of the Complex Ginzburg Landau equations. To adapt the theoretical CGL equations to the experimental conditions, specific hypothesis should be considered. In this study the experimental results are focused on the small growth of perturbations near the threshold when the amplitude of right and left waves are stationary [Fig. 2(a)]. Therefore, CGL equations are restricted to the case in which $\partial A/\partial t=0$, and linear and nonlinear coefficients of dispersion $c_i, i=0,1,2$ are ignored.

B. Extraction of CGLE coefficients

Real coefficients of Eq. (2) are extracted from spatiotemporal diagram of spirals using the demodulation technique with a Hilbert Transform to analyze the space-time diagrams of the pattern signal $I(z,t)$. The Hilbert Transform technique [31], consists of a first Fast Fourier Transform of the original signal $I(z,t)$ which is filtered in space with relatively large band; this allows the elimination of large-scale lighting inhomogeneities and small-scale noise. In the spectral space, the components of negative frequencies are set to zero with a smooth filter. After a bandpass filter with a band carefully adapted to each pattern, centered on the rolls frequency, an inverse Fourier Transform is applied to the truncated signal. For the clarity of the paper, we describe the technique for the right spiral; a similar procedure is applied for the left spiral. The real signal of the right spirals $|A(z,t)|$ is transformed in its complex equivalent expression as follows:

$$A(z,t)=|A(z,t)|e^{i\Phi(z,t)}. \quad (6)$$

The space-time diagram of amplitude $|A(z,t)|$ and the total phase $\Phi(z,t)$ are analyzed separately. The wave numbers and frequencies are determined as the spatial and temporal phase gradients:

$$q(z,t)=\partial\Phi/\partial z. \quad (7)$$

$$\omega(z,t)=2\pi f=\partial\Phi/\partial t. \quad (8)$$

Spatiotemporal diagram of spirals near the threshold [Fig. 2(a)] shows a source which separates right and left spirals. In the region of right spirals, the particular solution Eq. (4), substituted into the real part of the CGL Eq. (2), leads to the following equations for amplitude $A(q_p^2)$ and frequency $\omega_p(q_p)$ at equilibrium.

$$|A_q|^2=\frac{\varepsilon-\xi_0^2q_p^2}{g} \quad (9)$$

$$\omega_p=2\pi f_p=-v_gq_p= \quad (10)$$

To extract experimentally the CGLE coefficients from the spatiotemporal diagrams of spirals ($|A(z,t)|$), we have used the procedure developed Burguette *et al.* for hydrothermal wave patterns [30]. At each point i of the real spatiotemporal diagram, we have computed the amplitude $|A|(z_i,t_i)$, the wave number and frequency as follows:

$$q(z_i,t_i)=\partial_z\Phi; \quad \omega(z_i,t_i)=-\partial_t\Phi. \quad (11)$$

Several points have identical wave number with different values of amplitude and frequency. Statistical modes of amplitude A and frequency $f_p=\omega_p/2\pi$ are classified for each class q_{pR}. All modes are plotted versus the perturbed wave number q_{pR} in Figs. 3(a) and 3(b). The variation of $|A|$ with q_p is shown in Fig. 3(a). Experimental data of Fig. 3(a), plotted in term of $A^2(q_p^2)$ are compared with theoretical Eq. (9). At $q_p^2=0$ the amplitude Eq. (9) becomes $|A_q|^2=\varepsilon/g$. From the experimental data of Fig. 3(a) the nonlinear coefficient g is extracted. The slope of the curve $A^2(q_p^2)$ allows measurement of the value of $-\xi_0^2/g$ and extraction of the coherence length ξ_0.

The experimental value of axial group velocity v is obtained from Fig. 3(b) as the slope of the linear part of dispersion curve $\omega_q(q)=vq$. The group velocity determines the propagation of small perturbations.

To measure the characteristic time τ_0, we have used the dynamics of pattern in the neighborhood of the source in the spatiotemporal diagram. The characteristic time of the Interpenetrating Spirals is defined as the time needed for the system to generate the first spirals when the critical control parameter is reached. Near the threshold (in presence of the single source), the pattern has soft boundary conditions, so we can neglect the term $\partial^2A/\partial z^2$ and the nonlinear term. The resulting equation is

$$\tau_0v\frac{\partial A}{\partial z}=\varepsilon A. \quad (12)$$

with its corresponding solution

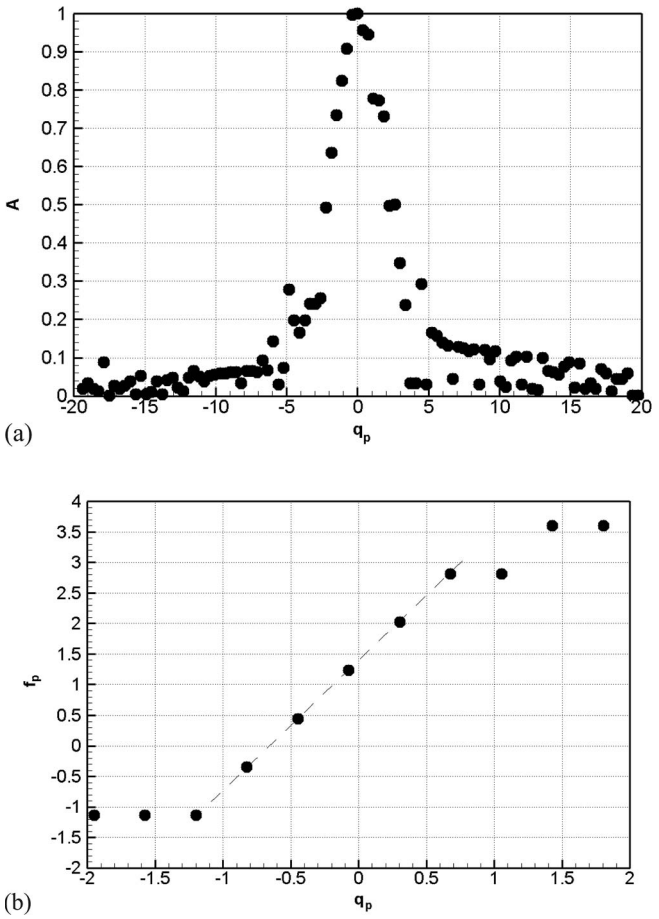

FIG. 3. Variation of amplitude (a) and frequency (b) of perturbations versus q_p for $R_o=-1200$ and $\varepsilon=0.012$.

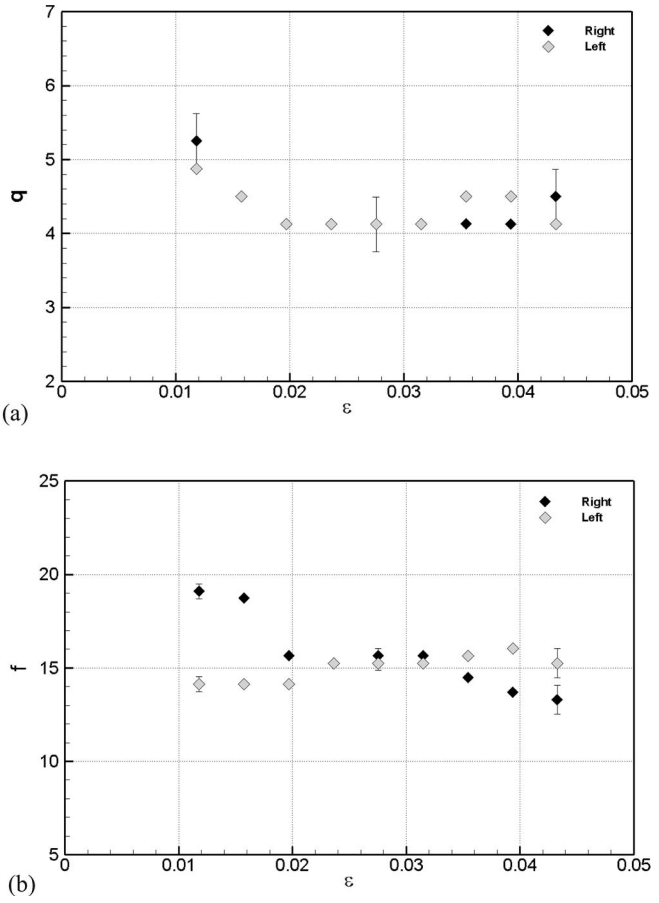

FIG. 4. Fundamental wave number (a) and frequency (b) of interpenetrating spirals versus ε for a fixed outer Reynolds number $R_o=-1200$.

$$ln\left(\frac{A}{A_0}\right)=\frac{\varepsilon}{\tau_0 v}z. \tag{13}$$

As the value of v has been determined before, one deduces the characteristic time τ_0 using the Eq. (13). The coefficient g, ξ_0, v, and τ_0 are extracted for the right spirals. Similar process is used for measuring the corresponding left spirals coefficients.

Measuring the coupling coefficient δ required particular attention to region of space-time diagram where both spirals coexist together [such as region three in Fig. 2(b)]. It should be noticed that the measurement of δ is valid only if the region of interpenetrating spirals remains stationary in time. It is very difficult to find such regions as right and left spirals travel in the system with a small difference in their frequency and wave number. Using previous coefficients for left and right spirals, (g, ξ_0, v, and τ_0), the real part of Ginzburg-Landau equations are applied to a spatiotemporal diagram where both spirals coexist. An estimated value of coupling coefficient δ is given in the next section.

IV. RESULTS

All coefficients are measured for a range of control parameter $0<\varepsilon<0.05$ for three value of fixed outer Reynolds numbers $R_o\in\{-1200,-1500,-2000\}$. For a fixed outer Reynolds number $R_o=-1200$, the first instability of the base flow occurs at critical value of the control parameter $R_{ic}=480$ and gives rise to a pattern of traveling left or right spirals: no hysteresis has been observed when ramping up and down. In order to study the behavior of spirals near the threshold, the wave number and fundamental frequency of right and left spirals are measured versus ε. As shown in Fig. 4(a), from $0<\varepsilon<0.02$ the wave number of both spirals decrease slightly reaching a constant value of $q=2\pi d/\lambda=4$, where $\lambda=0.929$ cm is the pattern wavelength. For $\varepsilon>0.02$ the characteristics of the flow changes. The interpenetrating spirals travel in the system with a constant wave number. A similar characteristic is observed for the fundamental frequency [Fig. 4(b)]. Near the threshold $0<\varepsilon<0.02$, because of the difference in their axial extent, left and right spirals have different frequencies which converge slightly to common value $f=d^2f_{dim}/\nu=15$ with $f_{dim}=0.43Hz$ for $\varepsilon\in]0.02,0.032[$.

A. Characteristic time scale (τ_0)

The characteristic time scale τ_0 is measured for different values of outer Reynolds numbers (Fig. 5). It is approxi-

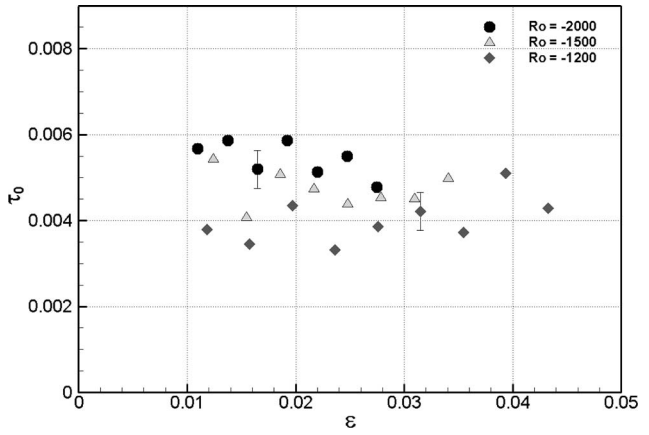

FIG. 5. The relaxation time versus ε.

mately constant versus ε and it is sensitive to values of R_o. For $R_o=-1200$, the average value of τ is $\tau_0=4.10^{-3}$ leading to a relaxation time $\tau=\tau_0/\varepsilon=0.2$ for $\varepsilon=0.02$.

B. Coherence length (ξ_0)

Extended systems contain a high degree of nonlinear competition of linearly unstable modes, due to the presence of boundaries, which break the original symmetries of the system. We have observed that near the walls, amplitude of counterpropagating spirals and interpenetrating spirals always vanished. The influence of boundaries is expressed using the comparison between the linear size of the system L with the coherence length ξ_0. To investigate the influence of control parameters on the coherence length, we have plotted in Fig. 6 the measured value of ξ_0 versus ε, for three different values of R_o. As shown Fig. 6, the coherence length ξ_0 is approximately constant versus ε but it increases with R_0. The right and left waves have approximately the same coherence length with similar behavior versus inner Reynolds number. For $R_0=-2000$ and $\varepsilon=0.02$, we have $\xi=\xi_0/\varepsilon^{1/2}=0.28$, which is comparable to $1/q_0=0.234$ where q_0 is the average wave number. Therefore $\xi_0<1/q_0\ll\Gamma$, this confirms the extendedness of the flow system.

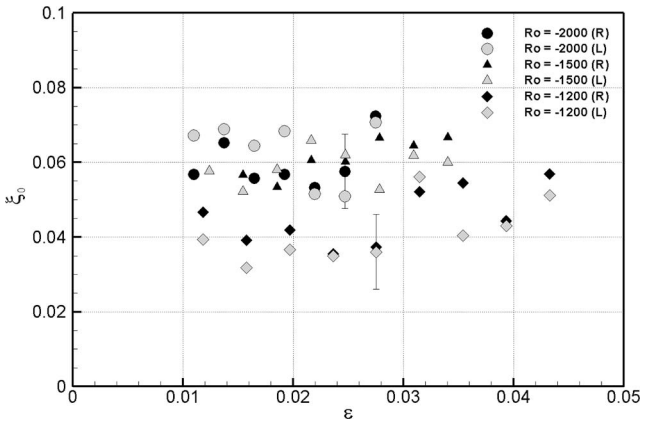

FIG. 6. The coherence length versus ε.

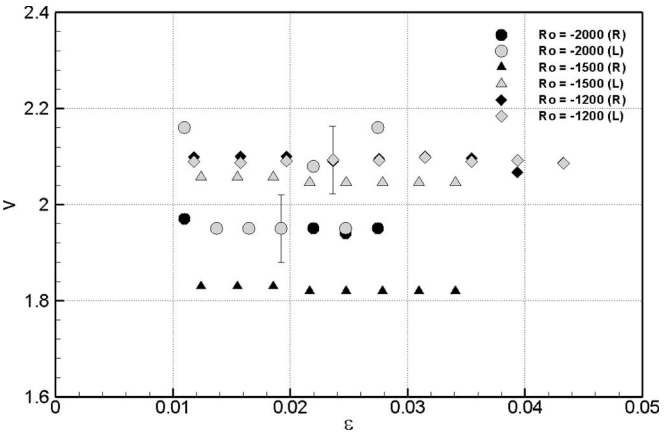

FIG. 7. The velocity group v versus ε.

C. Group velocity (v)

The axial group velocity is measured versus ε and presented in Fig. 7. It is constant versus ε and has approximately the same value for different values of the outer Reynolds number $R_o=-1200$ and $R_o=-2000$. However, it can be observed that the right spirals for $R_o=-1500$ has lower velocity group compared to the others. This difference could be related to the transient nature of the corresponding state. The values of the group velocity ($v\sim 2$) are very small compared to those of the phase velocity $c=2\pi f/q\sim 24$.

D. Nonlinear saturation coefficient (g)

The measured value of the nonlinear saturation coefficient g is plotted versus ε for three different values of the outer Reynolds number (Fig. 8). As shown in Fig. 8, the nonlinear saturation coefficient g increases with ε: $g(\varepsilon)=a\varepsilon+g_0$, where the values of the slope a for few values of R_o are given in the Table I.

The dependence of the coefficient g upon the external Reynolds number (Fig. 8) is more pronounced for $R_o=-2000$ than for $R_o=-1200$ or $R_o=-1500$. However, the slope of the nonlinear saturation coefficient is higher for $R_o=-2000$.

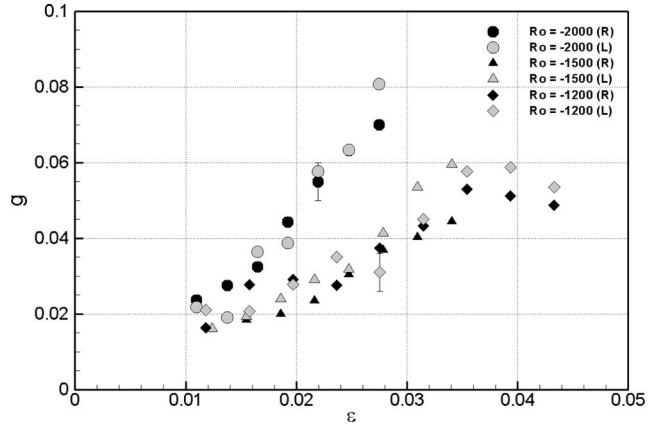

FIG. 8. The nonlinear saturation coefficient versus ε.

TABLE I. Slope of the nonlinear coefficient for values of R_o.

R_o	a_L	$10^3 g_{0L}$	a_R	$10^3 g_{0R}$
−1200	1.46	0.60	1.35	1.3
−1500	2.04	1.30	1.52	7.20
−2000	3.73	2.60	3.02	13.0

E. Coupling coefficient (δ)

As has been discussed before, the coupling coefficient δ could be measured only if the region of interpenetrating spirals remains stationary in time. This condition requires the selection of a specific spatiotemporal diagram where both spirals are traveling with exactly same wave number and frequency. It is, therefore, very difficult to measure the value of δ. The coupling coefficient δ was measured for only one case where $R_o=-2000$ and $\varepsilon=0.012$. The estimated value is $\delta=0.018$. It should be noticed that coefficient of coupling is comparable to the value of the nonlinear saturation coefficient $g=0.021$.

V. DISCUSSION

Table II gives values of the determined coefficients for $\varepsilon=0.012$. The knowledge of the coefficients of the Ginzburg-Landau equation is of great importance in the description of the pattern in extended systems with fixed boundaries. In fact, these coefficients enter into the scaling units of length, time, group velocity, and amplitude as follows:

$$z \to \frac{\varepsilon^{1/2}}{\xi_0} z, t \to \frac{\varepsilon}{\tau_0} t, v \to \frac{\varepsilon^{1/2}}{\xi_0} \tau_0 v, A \to \left(\frac{g}{\varepsilon}\right)^{1/2} A \qquad (14)$$

in order to reduce the CGLE to the form:

$$\frac{\partial A}{\partial t} + v\frac{\partial A}{\partial z} = A + (1+ic_1)\frac{\partial^2 A}{\partial z^2} - (1+ic_2)|A|^2 A. \qquad (15)$$

The scaled domain length becomes $l=L\varepsilon^{1/2}/\xi_0$. So in order to compare experimental results with numerical simulations from Eq. (14), one has to rescale the corresponding variables, depending on boundary conditions used in simulations. One should recall that for patterns in finite length domains or in the presence of counter-proapagating waves, the Galilean invariance is not valid and the group velocity cannot be eliminated from the single CGLE equation or the coupled system of CGLE equations [34,35].

The analysis of the behavior of real coefficients of Ginzburg-Landau equation helps to understand the influence of the control parameters on the counter-rotating Couette-Taylor flow. Previous experimental studies [5,6,12] were focused on different role of inner and outer rotating cylinders on the dynamics of intermittency regimes in the Couette-Taylor system. In their theoretical and numerical studies, Coughlin *et al.* [4] observed that the radial field velocity is separated by a nodal surface where the velocity is zero. This nodal surface divides the radial velocity profile into an inner region with a centrifugal instability and an outer region where the flow is stable. They conclude that the centrifugal instability is very active near the inner cylinder and the growth rate of the finite amplitude perturbations is stratified in the radial direction. The present results complement the previous paper as it discusses the influence of inner and outer parameters on the interpenetrating spirals flow which represents the first instability appearing before the intermittency regimes.

TABLE II. Experimental values of Ginzburg-Landau coefficients for $\varepsilon=0.012$.

R_o	$10^3\tau_0$	v	$10^2\xi_0$	$10^2 g$	$10^2\delta$
−1200	3.8	2.09	4.6	1.6	
−1500	5.4	2.06	5.7	1.6	
−2000	5.5	2.16	5.6	2.1	1.8

When the inner control parameter R_i increases in the system, the linear properties of the perturbations (the coherence length ξ_0, the group velocity v and the characteristics time τ_0) remain constant while the nonlinear coefficient g increases linearly with a slope depending on R_o (Table I). The increase in the inner Reynolds number R_i amplifies the nonlinear interaction of perturbations in the unstable zone close to it without changing sensitively its extent since the coherence length does not vary with R_i. The variation of the saturation coefficient with the criticality $g(\varepsilon)$ has been addressed in the theoretical study by Eckhaus *et al.* [36]. The variation of the slope with R_o can be linked to the structure of the flow for different external Reynolds number. In the stability diagram published by Andereck *et al.* [1] the transition from interpenetrating spirals to turbulent bursts appear for external Reynolds numbers −1200 and −1500 (for a constant inner Reynolds number $R_i=488$). However, for the same inner Reynolds ($R_i=488$), the transition is different for external Reynolds number $R_o=-2000$. At $R_o=-2000$ when the critical values of inner Reynolds number is reached, the interpenetrating spirals are suddenly replaced by turbulent spirals in the system. For a given value of R_i, the outer control parameter R_o has a sensitive influence on the linear and nonlinear coefficients of the Ginzburg-Landau equation. This is due to the variation of the unstable zone with the rotation of the outer cylinder.

Previous experimental results [8] concluded that the amount of perturbations in the system depends on the boundary condition at both sides of the system. It was observed that when boundary conditions rotate with the external cylinder the flow is more stable. This condition is satisfied in our experimental setup. Therefore the influence of rotating boundary conditions (rotating with the outer cylinder) are expressed through the coherence length which depends on the outer Reynolds number and remains constant with the increase of inner Reynolds number. The obtained results are therefore consistent with previous experimental results as the coherence length increases with the increase in perturbations, generated from the boundaries of the system. Recent studies [19,21] have shown that Ekman cells have influence in the formation of the Taylor vortices when the outer cylinder is at rest; no known similar theoretical and numerical studies are available in the case of counter-rotating cylinders and the

role of Ekman cells on the spiral vortices. In that case the flow induced by rotating the endplates attached to the outer rotating or inner rotating cylinder is more complex.

The behavior of sources in the transient state of IPS permits us to understand how waves appear in the system. The spatial and temporal stability of sources shows that both waves appear in the system with same value of wave number and slightly different frequency. Therefore the coupling phenomenon between the right and left waves is important. However, the short lifetime of sources shows that the coupling phenomenon collapses rapidly because each wave travels independently in the system (IPS). Furthermore, the rotation velocity of the inner cylinder increases, the lifetime of sources diminishes, and the coupling coefficient becomes rapidly negligible.

This result gives an idea about the behavior of the coupling coefficient δ which is difficult to determine experimentally in the system.

VI. CONCLUSION

The coupled complex Ginzburg-Landau equations is used to describe the dynamics of interpenetrating spirals in the counter-rotating Couette-Taylor system. The real coefficients of Ginzburg-Landau equations have been measured and their variation with the flow control parameters has been clarified. While the linear coefficients do not vary with R_i, the nonlinear saturation coefficient increases linearly with R_i for each investigated value of R_o. The variation of the saturation coefficient with the criticality $g(\varepsilon)$ is an important property that should lead to results in the numerical studies of the amplitude equations.

ACKNOWLEDGMENTS

This work was partially supported by the CPER Haute-Normandie. The authors have benefited from fruitful discussions with J. Burguette and A. Chiffaudel.

[1] C. D. Andereck, S. S. Liu, and H. L. Swinney, J. Fluid Mech. **164**, 155 (1986).
[2] P. Chossat and G. Iooss, *The Couette-Taylor Problem* (Springer-Verlag, Berlin, 1994).
[3] R. Tagg, Nonlinear Sci. Today **4**(3), 1 (1994).
[4] K. Coughlin and P. S. Marcus, Phys. Rev. Lett. **77**, 2214 (1996).
[5] I. Mutabazi, A. Goharzadeh and P. Laure, *The Physics of Rotating Fluids*, Lecture Notes in Physics Vol. 102 (Springer, New York, 2000).
[6] A. Goharzadeh and I. Mutabazi, Eur. Phys. J. B **19**, 157 (2001).
[7] C. Van Atta, J. Fluid Mech. **25**, 495 (1966).
[8] J. J. Hegseth, C. D. Andereck, F. Hayot, and Y. Pomeau, Phys. Rev. Lett. **62**, 257 (1989).
[9] H. Litschke and K. G. Roesner, Exp. Fluids **24**, 201 (1998).
[10] A. Prigent, G. Gregoire, H. Chate, O. Dauchot, and W. van Saarloos, Phys. Rev. Lett. **89**, 014501 (2002).
[11] D. Barkley and L. S. Tuckerman, Phys. Rev. Lett. **94**, 014502 (2005).
[12] A. Goharzadeh and I. Mutabazi, Eur. Phys. J. B **66**, 81 (2008).
[13] I. Hargittai and C. A. Pickover, *Spiral Symmetry* (World Scientific, Singapore, 1992).
[14] A. Schulz and G. Pfister, *The Physics of Rotating Fluids, 37 Lecture Notes in Physics* (Springer-Verlag, Berlin, 2000).
[15] W. F. Langford, R. Tagg, E. J. Kostelich, H. L. Swinney, and M. Golubitsky, Phys. Fluids **31**, 776 (1988).
[16] O. Czarny, E. Serre, P. Bontoux, and R. M. Lueptow, Theor. Comput. Fluid Dyn. **16**, 5 (2002).
[17] Ch. Hoffmann, M. Lucke, and A. Pinter, Phys. Rev. E **72**, 056311 (2005).
[18] A. Pinter, M. Lucke, and Ch. Hoffmann, Phys. Rev. Lett. **96**, 044506 (2006).
[19] J. Abshagen, O. Meincke, G. Pfister, K. A. Cliffe, and T. Mullin, J. Fluid Mech. **476**, 335 (2003).
[20] P. Manneville, *Dissipative Structures and Weak Turbulence* (Academic Press, Boston, 1990).
[21] P. Manneville and O. Czarny, Theor. Comput. Fluid Dyn. **23**, 15 (2009).
[22] M. C. Cross and P. C. Hohenberg, Rev. Mod. Phys. **65**, 851 (1993).
[23] W. van Saarloos, Phys. Rep. **386**, 29 (2003).
[24] S. Zaleski, P. Tabeling, and P. Lallemand, Phys. Rev. A **32**, 655 (1985).
[25] H. U. Voss, P. Kolodner, M. Abel, and J. Kurths, Phys. Rev. Lett. **83**, 3422 (1999).
[26] M. van Hecke, C. Storm, and W. van Saarloos, Physica D **134**, 1 (1999).
[27] I. Aranson and L. Kramer, Rev. Mod. Phys. **74**, 99 (2002).
[28] P. Kolodner, D. Bensimon, and C. M. Surko, Phys. Rev. Lett. **60**, 1723 (1988).
[29] P. Kolodner, Phys. Rev. A **46**, 6431 (1992).
[30] J. Burguete, H. Chate, F. Daviaud, and N. Mukolobwiez, Phys. Rev. Lett. **82**, 3252 (1999).
[31] P. Bot and I. Mutabazi, Eur. Phys. J. B **13**, 141 (2000).
[32] R. Tagg, W. S. Edwards, H. L. Swinney, and P. S. Marcus, Phys. Rev. A **39**, 3734 (1989).
[33] D. Walgraef, *Spatio-Temporal Pattern Formation* (Springer-Verlag, New York, 1997).
[34] L. Nana, A. B. Ezersky, and I. Mutabazi, Proc. R. Soc. London, Ser. A **465**, 2251 (2009).
[35] A. Nazarovsky, A. B. Ezersky, and I. Mutabazi, Proc. SPIE **5975**, 59750Y (2006).
[36] W. Eckhaus and G. Iooss, Physica D **39**, 124 (1989).